Current Research in Green and Sustainable Chemistry 5 (2022) 100305

Contents lists available at ScienceDirect

Current Research in Green and Sustainable Chemistry

journal homepage: www.elsevier.com/journals/current-research-in-green-and-sustainable-chemistry/2666-0865

Conversion of xylose to bioproducts on bifunctional supported platinum-group metals catalysts

Paola C. Oliveira [a], Simone J. Canhaci [b], Catarine B. Gabriel [b], Carla R. Moreira [b], Andréa M. Duarte de Farias [b], Marco A. Fraga [a,b,*]

[a] Instituto Militar de Engenharia, Praça Gen. Tibúrcio, 80, Urca, Rio de Janeiro, RJ, 22290-270, Brazil
[b] Instituto Nacional de Tecnologia – INT, Laboratório de Catálise, Av. Venezuela, 82/518, Saúde, Rio de Janeiro, RJ, 20081-312, Brazil

ARTICLE INFO

Keywords:
Hemicellulose
Pentose
Furfuryl alcohol
Lignocellulosic biomass
Green chemistry
Biomass conversion

ABSTRACT

Nb_2O_5-supported platinum-group metals catalysts were investigated in the one-pot aqueous-phase isomerization-dehydration-hydrogenation cascade conversion of xylose. The interplay between Nb_2O_5 acid sites and noble metal particles was discussed with a particular focus on catalyst stability. Pt/Nb_2O_5 was the best-performing catalyst for xylose upgrading regarding xylose consumption rates and high selectivity to furfuryl alcohol. It was chemically stable as no metal leaching to the aqueous phase was observed. Deposition of carbonaceous materials was identified as the main cause of deactivation and it disturbed the Brønsted acid sites in a more significant way. The impact of choosing an organic co-solvent was also demonstrated. Catalytic activity and distribution of bioproducts were determined by the organic solvent:water mixture. While polarity influenced activity, intermolecular interactions were suggested to tune selectivity.

1. Introduction

Upgrading waste lignocellulosic biomass to biofuels and bio-based chemicals is a key point towards the establishment of a bioeconomy. The development of suitable technologies able to forward this largely available renewable carbon source to a target bioproduct in a biorefinery deserves then special attention. Converting cellulose, hemicellulose and lignin, the three major fractions in lignocellulose biomass, is very challenging since these feedstocks considerably differ from those traditionally upgraded in oil refineries. They are very reactive hydrophilic compounds with low volatility that needs, consequently, to be processed in the liquid-phase at mild operation temperatures. More specifically, aqueous-phase processing (APP) is the most appropriate technology to be pursued as the monosaccharides are already released in water during cellulose and hemicellulose hydrolysis steps [1].

Cellulose hydrolysate can be fermented to second generation (2G) ethanol, which indeed has already been industrially made in Brazil [2]. It follows the Brazilian government policy on biofuels [3] and increases the overall production of ethanol, largely used in the country either blended with gasoline or directly in flex fuel vehicles. Producing 2G ethanol thus meets economical, environmental and social needs towards a more sustainable economy. Hemicellulose hydrolysate, on the other hand, is discarded as pentoses are not easily fermented [2], requiring a more expensive approach if producing hemicellulose-derived biofuels is aimed. Therefore, converting hemicellulose sugars into high valued green chemicals is appealing and can potentially contribute to design a more cost-effective decarbonization strategy.

Xylose is the most commonly found individual sugar in hemicellulose hydrolysates due to the prevalence of xylans in most hemicelluloses despite the differences in composition according to the biomass source [4]. Concentrations of xylose in xylan-rich sugarcane hemicellulose hydrolysate are usually low (80–160 mmol L^{-1}) [5] and depend on the pre-treatment the biomass is submitted to in 2G ethanol production process. Over the last years, some efforts have been made to convert such low-concentration xylose aqueous solution into several chemicals, mainly xylitol, furfural, furfuryl alcohol and levulinic acid/alkyl levulinates [6–12]. Each of those target chemicals presents their specific challenges as concerning catalyst development. While xylitol and furfural are produced through a single reaction step, either hydrogenation or dehydration, one-pot formation of furfuryl alcohol and levulinic acid/alkyl levulinates relies on cascade reactions and demands multiple and distinctive active sites [13]. Coupling xylose dehydration and furfural hydrogenation reactions to produce furfuryl alcohol requires either a dual catalytic system [6,14] or a bifunctional acid-metal catalyst [7,8,15].

* Corresponding author. Instituto Militar de Engenharia, Praça Gen. Tibúrcio, 80, Urca, Rio de Janeiro, RJ, 22290-270, Brazil.
E-mail address: marco.fraga@int.gov.br (M.A. Fraga).

https://doi.org/10.1016/j.crgsc.2022.100305
Received 29 December 2021; Received in revised form 8 March 2022; Accepted 27 March 2022
Available online 29 March 2022

Furfuryl alcohol is a strategic hemicellulose-derived chemical as it is used in different chemical industries to manufacture lubricant, plasticizers and dispersing agent [16], as a fine chemical intermediate for producing vitamin C and lysine [17] and to obtain levulinic acid and 2-methylfuran, a prospective biofuel or fuel bioadditive [18]. Perez and Fraga first reported the one-pot furfuryl alcohol synthesis over a sulphated zirconia-Pt/SiO_2 dual catalytic system reaching selectivity of 55% [6]. Recovery and regeneration of both catalysts revealed to be difficult, hampering the feasibility of an industrial-scale use. Assembling a single bifunctional catalyst has also been shown challenging and the stability of acid sites is now known to be a crucial factor [7,8]. Indeed, furfuryl alcohol selectivity of around 90% was accomplished at 130 °C over an organic-inorganic hybrid acid-metal catalyst at which acidity was provided by grafted –SO_3H groups while Pt nanoparticles were the hydrogenating centers [8]. Nonetheless, hydrolysis of such surface acid moieties led to catalyst deactivation upon consecutive reaction cycles also affecting product distribution with a marked decrease in furfuryl alcohol selectivity. Using sulphated zirconia as support instead rendered no different performance as regarding catalyst stability [7]. Another relevant drawback of both approaches is the sulfur released to the aqueous media contaminating the bio-based end products and thus jeopardizing the overall process sustainability.

Multiwalled carbon nanotubes (MWCNT) functionalized with acidic oxygen surface groups and decorated with Pt, Pd, Ru, Rh and Au nanoparticles were then recently investigated [9]. Despite the high activity of those catalysts and the stability of the oxygenated surface groups on MWCNT under mild xylose APP conditions, bringing an important advantage over previously studied sulfur-containing acidic groups [7,8] xylose was mainly converted to xylitol providing up to 85% yield. Furfuryl alcohol was also produced but selectivity did not exceed 20% over Pd and Rh-based catalysts, being even lower over the other supported metals. This poor performance to promote the cascade reactions was associated with the concentration and acid strength of surface sites on MWCNT generated by liquid-phase oxidation [9]. The susceptibility of oxygenated acid groups on carbon surface to hydrolysis in hot liquid water was, however, reported under harsher biomass conversion conditions [19] and it should then be carefully considered when acidic carbon materials are taken for designing biomass aqueous-phase valorization catalysts.

It stands clear from those results [6–9] that promoting one-pot aqueous-phase dehydration-hydrogenation cascade conversion of xylose to furfuryl alcohol is still an open challenge as no catalyst holding stable metal and acid sites with a proper acidity strength was presented so far. In this contribution, Nb_2O_5-supported platinum-group metals (Pt, Pd, Ru and Rh) catalysts are systematically investigated for such purpose. The interplay between Nb_2O_5 acid sites and noble metal particles is discussed with a particular focus on the catalyst stability. The impact of choosing a suitable organic co-solvent is also well demonstrated.

2. Materials and methods

2.1. Catalyst preparation

Niobium oxide (CBMM) was used as support for metal supported catalysts prepared by incipient wetness impregnation, generating M/Nb_2O_5 samples with approximately 1 wt% M loading, where M = Pt, Pd, Ru or Rh. Initially, Nb_2O_5 was calcined in static atmosphere at 400 °C for 5 h (10 °C min^{-1}) before the addition of the aqueous solutions of the metal precursor salts: $[Pt(NH_3)_4(NO_3)_2]$, $[Pd(NH_3)_4(NO_3)_2]$, $RuCl_3.3H_2O$ and $Rh(NO_3)_3$. After impregnation, samples were dried at 80 °C for 18 h and calcined in air (30 mL min^{-1}) at 400 °C for 2 h (10 °C min^{-1}).

2.2. Characterization of support and fresh catalysts

The specific surface area of the support was determined by nitrogen adsorption-desorption isotherms at −196 °C using a Micromeritics ASAP 2420 equipment, according to the Brunauer-Emmet-Teller (BET) equation. The solid was degassed before analysis at 400 °C for 24 h.

Metal loadings of the as-prepared catalysts were determined by inductively coupled plasma optical emission spectrometry (ICP-OES) in a PerkinElmer Optima 2100DV equipment. The procedures for the digestion of samples were based on ASTME 1552-15, ASTME 2371-13 and experimental protocols described elsewhere [20]. Briefly, around 100 mg of the sample were submitted to acid digestion with a solution composed of HF (3 mL), HCl 37% (1.5 mL) and HNO_3 60% (1.0 mL) while placed on a heating plate at 100 °C for 15 min. As for the Ru/Nb_2O_5 catalyst, it was carried out with the aid of a microwave oven. After, 10 mL of regal water (3:1 HCl:HNO_3) were added to conclude the digestion. Finally, the samples volume was completed up to 50 mL with a HNO_3 1% solution. To avoid any matrix interference, solutions of analytical standards used for calibrating the equipment were prepared with a Nb_2O_5 solution (500 mg of Nb_2O_5 in 15 mL of HF, 7.5 mL of HCl 37% and 5 mL of HF 60%, the volume brought to 250 mL with HNO_3 1% solution).

Electron microscopy images of all metal catalysts were collected after dispersing the solids in ethanol by ultrasonication and dropping the suspension on holey carbon-coated copper grids. Samples were also embedded in Spurr® resin followed by ultrathin sectioning (60 nm) with a RMC Boeckeler ultramicrotome (PT-PC), using a diamond knife. Micrographs were obtained by using the scanning transmission electron (STEM) mode in a field emission gun scanning electron microscope (FEG-SEM) – STEM-in-SEM – from FEI/Thermo Fischer (Helios Nanolab Dual Beam G3 CX), operating at 30 kV. Before the STEM-in-SEM analyses, catalysts were reduced under H_2, at 300 °C, for 1 h, and then passivated at −70 °C under 5%O_2/N_2 flow. Metal particle size measurements were performed by using Image-J software, version 1.52a. Around 200 particles were considered for each sample for statistical purposes. These data enabled the calculation of particle size distribution and metal dispersion (D) by considering the length-number mean diameter (d_m) based on Equations (1) and (2):

$$d_m = \frac{\sum n_i d_i}{\sum n_i} \quad (1)$$

$$D = 6\frac{v_m/a_m}{d_m} \quad (2)$$

where n_i is the number of spherical particles of diameter d_i, v_m is the volume of the metal atom and a_m the surface area occupied by an atom.

The amount of total acid sites was determined by ammonia temperature-programmed desorption (NH_3-TPD) in a Micromeritics Autochem 2920 equipment. All samples, support and metal catalysts, were pre-treated in situ at 400 °C, under air flow (30 mL min^{-1}) for 30 min. After, it was cooled down to 40 °C and purged with He (30 mL min^{-1}) for 30 min. The adsorption step was carried out at 100 °C, with a continuous flow of 4% NH_3/He (30 mL min^{-1}), for 30 min, to achieve saturation. Physically adsorbed molecules were removed by purging the reactor with He for 20 min (30 mL min^{-1}). For the desorption step, He was kept flowing while heating up the sample to 400 °C (20 °C min^{-1}). The samples were held at this final temperature for an additional 30 min.

Complementary infrared spectroscopy analysis of the support was performed using pyridine as a probe molecule (FTIR-Py) to identify the nature of surface acid sites. Prior to analysis, self-supported wafer of Nb_2O_5 was treated under vacuum at 400 °C for 1 h in a glass cell. Next, the wafer was cooled to room temperature, submitted to 10 Torr of pyridine for 30 min and degassed to remove non-adsorbed and physisorbed probe molecules. Infrared spectrum was collected within 400–4000 cm^{-1} in a Nicolet iS50 spectrometer. The concentration of Lewis and Brønsted acid sites per gram of catalyst was determined by the optical area of vibrations at around 1454 cm^{-1} and 1545 cm^{-1}, respectively, and corrected by the molar extinction coefficients [21].

Experimental metal loading collected from ICP-OES and metal dispersion (D) estimated from STEM images were taken to determine the

amount of surface metal sites (n_{MeS}) according to Equation (3):

$$n_{MeS} = \left(\frac{metal\ loading}{metal\ molar\ mass}\right) D \quad (3)$$

These data was used to calculate acid/metal molar ratio considering the concentration of acid sites derived from the quantitative NH_3-TPD analyses of the supported catalysts.

2.3. Catalyst evaluation

The liquid-phase conversion of xylose was first studied on Nb_2O_5-supported platinum-group metals (Pd, Pt, Rh and Ru). The catalysts were evaluated in a 300 mL batch reactor from Parr Instruments Company equipped with temperature and pressure control and mechanical agitation.

Before each run, catalysts were reduced under H_2 flow (30 mL min^{-1}) at 300 °C for 1 h. Reaction runs of 2, 4 or 6 h were conducted at 130 °C, under total pressure of 30 bar (P_{H2} = 25 bar), agitation of 600 rpm, 125 mg of catalyst. These conditions were preliminarily determined and were shown to avoid diffusional limitations and assure kinetic control. Xylose solutions at 83 mmol L^{-1} were prepared in organic solvent:water 1:1 mixtures using tetrahydrofuran (THF), isopropanol, tert-butanol, acetone and γ-valerolactone (GVL). Samples were collected at the end of each run after immediately cooling the reactor with the aid of an ice bath.

Products were analyzed by high performance liquid chromatography (HPLC) using a Waters E2695 Alliance equipment, with a Biorad Aminex HPX-87H column and an aqueous solution of H_2SO_4 (5 mmol L^{-1} and 0.7 mL min^{-1}) as eluent. The temperature of the column was kept at 65 °C and that of the RI detector at 50 °C. Products were identified by their retention times compared to available standards, which were also used to collect analytical curves. The aliquots were previously filtered with a 0.22 μm PVDF filter and analyzed in triplicate (error ≤5%).

Xylose conversion, products selectivity and carbon balance were determined as shown in Equations (4)–(6):

$$Conversion\ of\ xylose = \frac{\left([xylose]_0 - [xylose]_t\right)}{[xylose]_0} \times 100\% \quad (4)$$

$$Selectivity = \frac{[product]_i}{[xylose]_0 - [xylose]_t} \times 100\% \quad (5)$$

$$Carbon\ balance = \frac{\left(\sum [product]_i \times nCP_i\right)}{[xylose]_0 \times 5} \times 100\% \quad (6)$$

where $[xylose]_0$ is xylose initial concentration, $[xylose]_t$ is xylose concentration after reaction time, $[product_i]$ is the product concentration, nCP_i is the number of carbon atoms in product *i*.

Catalyst deactivation was assessed by running two consecutive catalytic runs. After the first run, the reaction medium was removed and the reactor was charged with a new xylose solution. These runs were carried out under the same conditions. Catalyst regeneration was assessed by submitting the spent sample to activation thermal treatment right after the two reaction cycles, which already revealed catalyst deactivation. The spent catalyst was initially calcined at 400 °C for 2 h (10 °C min^{-1}), then reduced following the same protocol applied for the fresh samples (300 °C, 10 °C min^{-1}, 1 h) and finally used in another reaction run.

2.4. Post-reaction analyses of spent catalysts

Spent Pt/Nb_2O_5 catalysts were recovered by filtration, washed and dried overnight at 100 °C. They were then characterized as regarding the carbon content by elementar CHN chemical analysis in a LECO CHN638 analyzer. The experimental methodology followed the protocols ASTM D5291 and ASTM D5373. As a reference, the freshly reduced catalyst was also analyzed. Thermogravimetric analysis was also performed on a NETZSCH STA 409 *Pc* Luxx equipment. The solid was heated up to 950 °C at a rate of 10 °C min^{-1} under 60 mL min^{-1} air stream.

The post-reaction liquid phases were analyzed by inductively coupled plasma optical emission spectrometry (ICP-OES) to assess the eventual presence of leached metal. These analyses followed the same experimental procedures and equipment described in the preceding experimental part for the fresh catalysts.

3. Results and discussion

The commercial Nb_2O_5 support and the supported platinum-group metals catalysts were characterized concerning only the main properties related to the targeted xylose upgrading reaction.

The support presented a high surface area (100 $m^2\ g^{-1}$) and this value is in agreement with data usually reported for similar commercial Nb_2O_5 powders [22–24]. Its total acidity was assessed by NH_3-TPD and the desorption profile presented in Fig. 1a exhibits only one broad desorption peak at 238 °C, indicating the occurrence of a wide distribution of acid sites with different strength in line with some previous reports [22]. The profile of Pt/Nb_2O_5 catalyst is very alike (Fig. 1a) holding a desorption peak at 230 °C. As for Ru, Rh and Pd based catalysts, besides this first broad peak at around 228–245 °C, a more resolved second desorption peak was also recorded at higher temperatures, 321 °C, 337 °C and 372 °C for Rh/Nb_2O_5, Pd/Nb_2O_5 and Ru/Nb_2O_5, suggesting that a higher concentration of more acidic sites is formed upon catalyst preparation. Total amount of acid sites was determined from these profiles as summarized in Table 1. The presence of higher temperature desorption peak has been described before [25] as well as an increase in catalyst total acidity when compared to the bare support [26].

Infrared spectrum of pyridine adsorbed on the support (Fig. 1b) showed absorption bands at 1448 and 1610 cm^{-1} that are typically ascribed to pyridine coordinated to Lewis acid sites. A smaller band at 1545 cm^{-1}, on the other hand, is associated with the formation of pyridinium ion by the coordination of pyridine molecules to Brønsted acid sites. Lastly, a vibration at around 1490 cm^{-1} was also registered and it raises due to the superposition of bands related to both Brønsted and Lewis acid sites [27].

These results reveal that the Nb_2O_5 used as support holds both Lewis and Brønsted acid sites even after calcination at 400 °C. Nb_2O_5 is indeed well reckoned by presenting both sort of acid centers whose occurrence is intimately related to the thermal treatment the oxide is submitted [28, 29]. Quantitative assessment of the support acidity allowed estimating a ratio between concentration of Brønsted and Lewis acid sites of 0.53.

Metal loadings and average particle size of all catalysts were determined and the results are collected in Table 1. They show that the metal contents are close to the corresponding nominal values while particle sizes range within 4.9–8.7 nm as determined from the STEM images (Fig. 2). These characterization results together show that the prepared catalysts indeed possess the acid and metal features required for promoting xylose cascade conversion to bioproducts. Hence, all bifunctional supported platinum-group metals catalysts were tested in batch mode liquid-phase xylose conversion under the same reaction conditions and the data are also summarized in Table 1.

Initially, two control experiments were performed to examine the eventual conversion of xylose in the absence of any catalyst and the activity of Nb_2O_5 taken as the acidic support.

Negligible non-catalyzed conversion of xylose (3%) was found under those conditions, allowing then to clearly examine the role played by the support and the catalysts. Running the reaction in the presence of bare Nb_2O_5 disclosed that the support itself is active for xylose conversion, leading mostly to furfural and a minor selectivity to xylulose (Table 1). It is very well known that xylose can be dehydrated to furfural over heterogeneous acid catalysts [30], particularly those holding both Lewis and Brønsted acid sites [31] as on the present Nb_2O_5 support (Fig. 1b). Xylulose is formed from xylose isomerization on Lewis acid sites [32,33], which is then readily converted to furfural [31,32,34]. The results

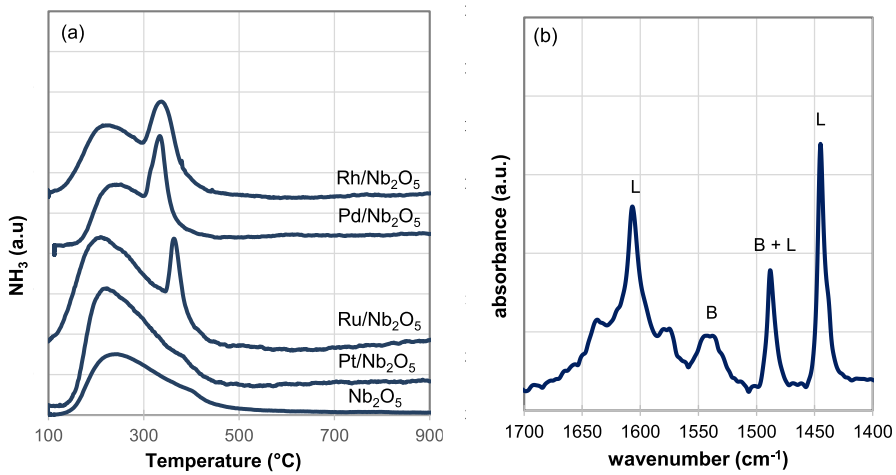

Fig. 1. NH_3 thermodesorption profile of all samples (a) and infrared spectrum of adsorbed pyridine on Nb_2O_5 (b).

Table 1
Metal loading, average metal particle size (d), concentration of catalyst acid sites, acid/metal sites ratio, reaction rates and selectivity to xylulose (xylu), xylitol (xOL), furfural (FF) and furfuryl alcohol (FFA). Reaction conditions: 130 °C, 30 bar (P_{H2} = 25 bar), THF:water 1:1, 2 h, C_{xylose} = 83 mmol L^{-1}.

Catalyst	Metal loading (wt.%)	d (nm)	Acid sites (μmol/g_{cat})	Acid/metal sites ratio	Reaction rate (mmol g_{cat}^{-1} h^{-1})	Reaction rate (mmol g_{met}^{-1} h^{-1})[a]	Conversion[b] (%)	Selectivity[c] (%)			
								xylu	xOL	FF	FFA
–	–	–	–	–	–	–	3	100	0	0	0
Nb_2O_5	–	–	286	–	89.1	–	33	13	0	83	0
Ru/ Nb_2O_5	1.34	8.7	344	17.5	99.4	7.4	31	18	0	31	19
Pd/ Nb_2O_5	1.20	4.9	288	11.4	104.8	8.7	33	16	3	6	42
Rh/ Nb_2O_5	1.26	8.0	291	17.5	106.9	8.5	33	19	4	8	22
Pt/ Nb_2O_5	1.05	6.6	276	30.0	132.1	12.6	36	18	6	24	43

[a] Mass-specific activity of active metal.
[b] conversion at which selectivity was calculated.
[c] Data at isoconversion (~30%).

presented herein show therefore that the acid sites on the Nb_2O_5 used as support are indeed able to promote such dehydration reaction. Accordingly, previous works in the literature reported on the activity of Nb_2O_5 for xylose dehydration either in water or water-organic solvent mixtures [24,35,36] and revealed that selectivity varies a lot according to the organic solvent and reaction temperature applied. Comparing to this study, Gupta et al. [36] reported a higher catalytic activity (99% conversion after 3 h) but a much lower furfural selectivity (44%) over Nb_2O_5 when water:THF 1:1.5 solvent mixture was used. These differences in the catalyst performance may be ascribed to the lower concentration of surface acid sites on the Nb_2O_5 sample (0.17 mmol g^{-1} in Ref. [36] versus 0.55 mmol g^{-1} in this study, both assessed by FTIR-Py).

The addition of a metal phase, irrespective of the platinum-group metal, completely changed product distribution despite a less important impact on catalytic activity as disclosed by the reaction rates (Table 1).

Besides xylulose and furfural, which were still formed, furfuryl alcohol raises as the major product especially over supported Pt and Pd catalysts that led to practically the same selectivity level. Selectivity to xylulose was low, ranging within only 16–19%, and it is a result of the support active Lewis acid sites as discussed hereinbefore.

Production of xylitol indicates that direct xylose hydrogenation on metal sites also takes place but it is plainly less important as the highest selectivity barely reaches 6% over Pt/Nb_2O_5. This performance contrasts with those previously reported by Perez et al. [9] at which selectivity to xylitol varied within 70–85% over 1D functionalized multiwalled carbon nanotubes (MWCNT)-supported noble metal catalysts under the same reaction conditions (130 °C, 30 bar and xylose initial concentration of 83 mmol L^{-1}). Xylose catalytic hydrogenation to xylitol is indeed generally promoted in the presence of a metal catalyst at temperatures between 80 and 140 °C and hydrogen pressures up to 50 bar [37]. Therefore, the results obtained over Nb_2O_5-supported catalysts in this present contribution can be taken as an indicative of the catalyst bifunctionality, i.e. that both acid and metal sites are cooperatively playing their roles hindering the direct hydrogenation to xylitol. Consequently, furfuryl alcohol formation is favored in a reaction cascade whereby xylose is dehydrated to furfural on the support acid centers and furfural is then hydrogenated on the metal sites as depicted in Scheme 1. The divergence with those data from Perez et al. [9] might be associated with the lower acidity of the functionalized MWCNT used as support.

Differences in performance were also observed amongst the Nb_2O_5-supported catalysts studied herein (Table 1) and they should be rationalized considering both sort of surface sites.

Nb_2O_5-supported Ru, Rh and Pd catalysts hold the same balance between acid and metal sites, unveiling that the nature of the metal phase is also pertinent. Furthermore, Pt/Nb_2O_5 holds a higher acid/metal ratio, around twice as high (Table 1), and it emerges as the one rendering the best result toward furfuryl alcohol. It would imply that xylose dehydration step could be favored by the higher density of acid sites compared to the metal sites; however, the higher specificity of Pt^0 sites on furfural hydrogenation led to a higher selectivity towards furfuryl alcohol than over the other supported noble metal samples. This assumption was

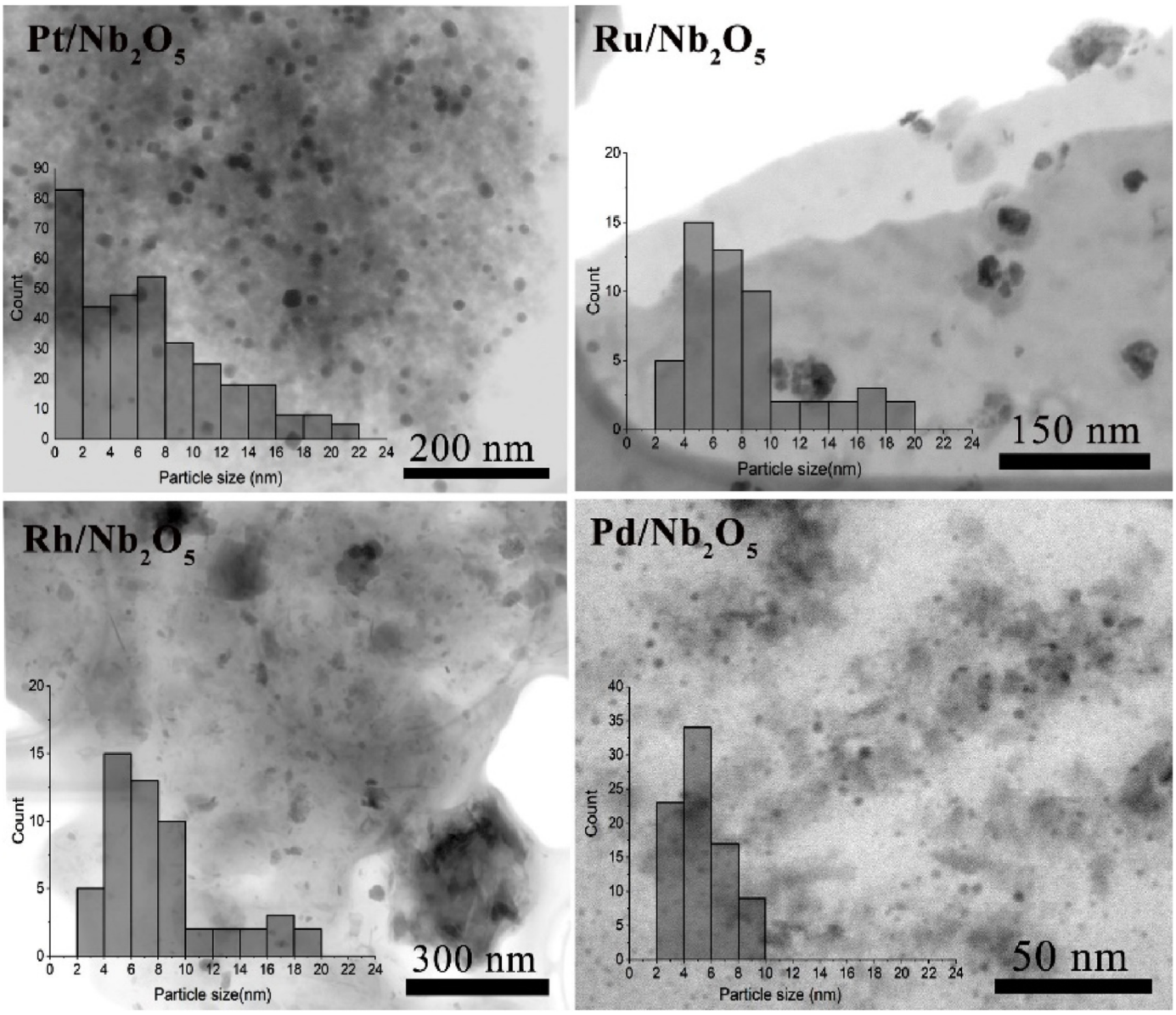

Fig. 2. Scanning transmission electron microscopy images and particle size distribution of all catalysts.

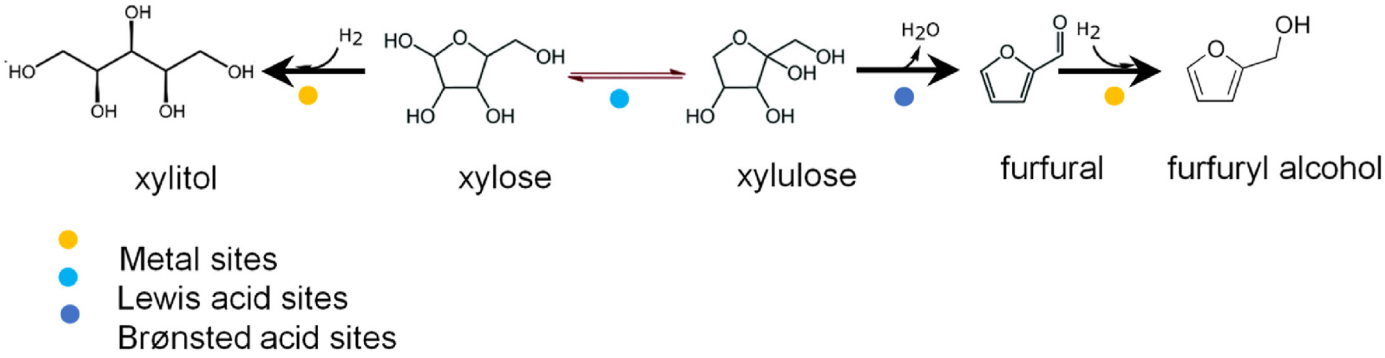

Scheme 1. Simplified reaction network for xylose upgrading over acid/metal bifunctional catalysts.

indeed confirmed when furfural was used as a feedstock instead of xylose under the same reaction conditions as displayed in Fig. 3. The performance of Ru/Nb_2O_5 was also examined to contrast the results and it corroborated our conclusion as it presented a much lower selectivity to C═O reduction.

Hydrogenation of the intermediate furfural on noble metal catalysts is known to lead to different chemicals as possible reaction pathways may involve hydrogenation, hydrogenolysis, decarbonylation and ring-opening reactions according to the metal distinct activity to a specific group, either C═O or C═C, and the role played by the support [38]. It

has been reported that reaction preferably proceeds on C═O group over Pt and Ru while C═C reduction occurs mainly on Pd-based catalysts [38,39]. Ru catalysts, however, have been found to lead the reaction further to 2-methylfuran by subsequent decarbonylation of furfuryl alcohol, particularly in the presence of Lewis acid sites provided by the support or Ru oxide species onto the catalyst surface [39,40]. Our results are in line with such reports and the capability of Ru to push the reaction to over hydrogenated products is clear by the large amount of other unidentified compounds formed.

Conclusively, the bifunctional Pt/Nb_2O_5 stands out as the best-performing catalyst for xylose upgrading not only regarding xylose consumption rates but it also produces much less byproducts. Indeed, reaction data in Table 1 show that selectivity to C5 products – xylulose, xylitol, furfural and furfuryl alcohol – sums 91% over Pt/Nb_2O_5 while it ranges from 68 to 53% for the other metals, disclosing a larger product diversity. This might be related to the lower selectivity of other noble metals to C═O hydrogenation as already discussed (Fig. 3). Nonetheless, the role played by the acidity should not be overlooked as it is known to promote polymerization and resinification reactions producing soluble and insoluble polymers [41–43].

The Pt/Nb_2O_5 catalyst was used to investigate the impact of the solvent mixture on catalyst performance and kinetics. It is widely known that the solvent can have a significant impact on liquid-phase catalyzed reaction, affecting feedstock conversion, product distribution, catalyst integrity, products separation and suppression of degradation side reactions. It has indeed been carefully investigated for xylose dehydration [41,44] and furfural hydrogenation [45,46] separate reactions. While polar aprotic solvents have been shown to significant increase reaction rate and furfural selectivity in xylose dehydration [44], furfural seems to be more easily hydrogenated on protic solvent [45,47], particularly strong polar solvents when furfuryl alcohol is the desired product [45,48].

Notwithstanding those studies, scarce information is available on the solvent impact on one-pot conversion of xylose to bioproducts [14,15,49]. In this present contribution, therefore, only polar and water-miscible organic solvents were examined. They were used in monophasic mixtures with water to guarantee xylose solubility and also because the technological targeted hemicellulose hydrolysate to be upgraded is available in large amounts of water, as low-concentration xylose aqueous solution as described hereinbefore.

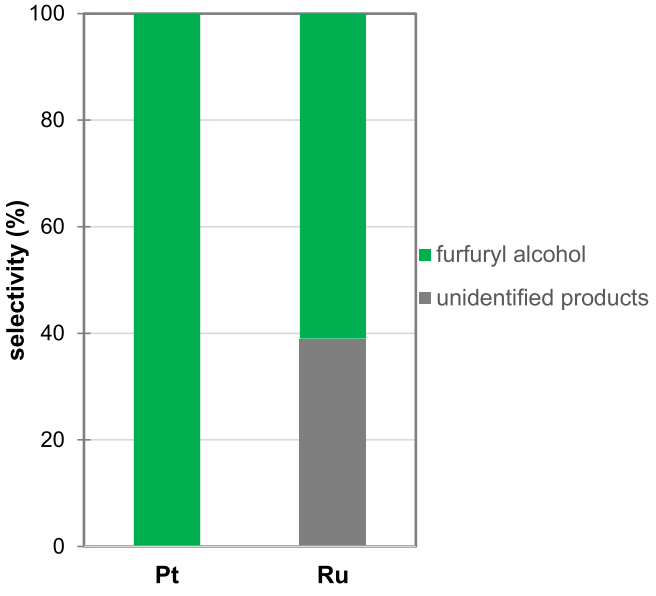

Fig. 3. Products selectivity from furfural hydrogenation over Nb_2O_5-supported Pt and Ru catalysts. Reaction conditions: 130 °C, 30 bar (P_{H2} = 25 bar), THF:water 1:1, 2 h.

Using organic solvent and water mixtures changed the catalyst performance as disclosed by the reaction data summarized in Table 2. Xylose conversion rate varied within 99.9–132.1 mmol g_{cat}^{-1} h^{-1} and it was found to decrease with the increase of solvent polarity (ε) irrespective of using a protic or aprotic polar solvent. The lowest overall activity was reached in pure water while the highest was accomplished in water:THF. Indeed, reaction rate correlated well with the solvent polarity described by the dielectric constant calculated for the organic solvent and water mixtures [50] as depicted in Fig. 4.

These results are in line with those reporting xylose uptakes either through dehydration or hydrogenation separate reactions on acid or metal catalysts, respectively. THF has been shown to meaningfully enhance acid-catalyzed formation of furfural compared to water [41] whereas the use of organic solvent increases hydrogenation rates due to the higher solubility of hydrogen [51,52]. Moreover, the organic solvents can also loose the interaction between water molecules and surface acid sites, which invariably weaken their catalytic activity [10,27,53].

Product distribution was also affected by the nature of the solvent mixture used, despite they all rendered mainly xylulose, xylitol, furfural and furfuryl alcohol. It is noted that the highest selectivity to furfuryl alcohol was also attained by using THF. Nonetheless, contrarily to the catalytic activity, no clear dependence with the solvent polarity was drawn. It is indeed easily noted since no furfuryl alcohol was produced when tert-butanol was used and it presents the second lowest polarity (ε = 10.90), followed by THF (ε = 7.58). Driving product distribution is likely to be ascribed to intermolecular interactions between solvent and xylose/bioproducts and the stabilization of reaction intermediates, particularly concerning the reduction of C═O groups in intermediate furfural.

Taking the ratio between furfuryl alcohol and furfural selectivity (S_{FFA}/S_{FF}) as a descriptor (Table 2), it is seen that a more balanced formation of those bioproducts was achieved with the protic solvents (pure water and isopropanol).

At this point, it is important to mention that no furfuryl alcohol formation takes place through transfer hydrogenation when isopropanol is used as organic solvent as depicted in Fig. 5, which depicts the products detected by HPLC analyses. It is seen that when the reaction is carried out under nitrogen pressure instead of hydrogen only xylulose and furfural are produced.

It is proposed that the balanced S_{FFA}/S_{FF} ratio is related to the hydrogen bonding between the carbonyl group in intermediate furfural and the solvent molecules preventing the aldehyde hydrogenation. It has indeed been shown before that such intermolecular interaction hinders C═O reduction while favoring the hydrogenation of the furanyl ring [40,47]. Tert-butanol, which is also a protic solvent, completely hindered the formation of furfuryl alcohol (S_{FFA}/S_{FF} = 0). It might be associated with the more effective shielding effect of larger tert-butanol molecules on the carbonyl group. It is important to outline, though, that both alcohols

Table 2
Solvents, reaction rate, product selectivity to xylulose (xylu), xylitol (xOL), furfural (FF) and furfuryl alcohol (FFA), and ratio between furfuryl alcohol and furfural selectivities (S_{FFA}/S_{FF}) of xylose conversion on Pt/Nb_2O_5. Reaction conditions: 130 °C, 30 bar (P_{H2} = 25 bar), 2 h.

Solvent	Reaction rate (mmol g_{cat}^{-1} h^{-1})	Selectivity[a] (%)				S_{FFA}/S_{FF}
		xylu	xOL	FF	FFA	
Water	99.9	26	13	22	33	1.5
GVL[b]	105.9	20	13	36	10	0.3
Isopropanol[b]	119.7	11	7	15	18	1.2
Acetone[b]	123.3	16	16	14	25	1.8
tert-butanol[b]	126.2	16	10	16	0	0
THF[b]	132.1	18	6	24	43	1.8

[a] Data at isoconversion (~30%).
[b] Organic solvent in 1:1 mixture with water.

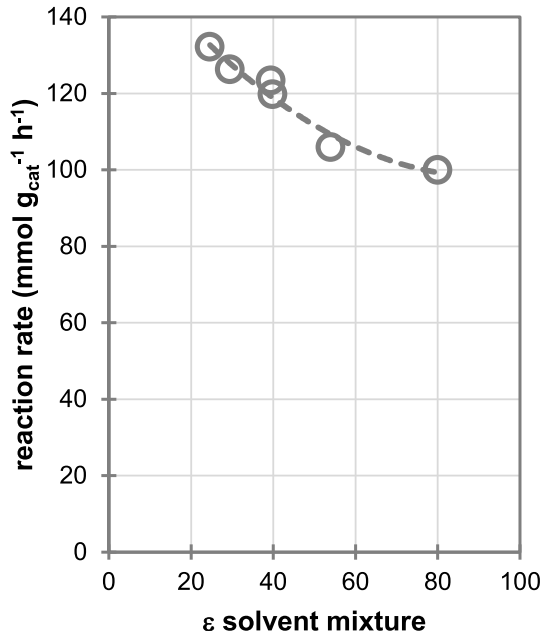

Fig. 4. Correlation between reaction rate over Pt/Nb_2O_5 and dielectric constant (ε) of organic solvent and water mixtures used as solvent. Reaction conditions: 130 °C, 30 bar (P_{H2} = 25 bar), organic solvent:water 1:1, 2 h.

(isopropanol and tert-butanol) also allowed the occurrence of undesired side reactions, rendering the lowest sum of all identified products in Table 2. It should be noted that alcohols can also interact with the acid sites on the catalyst surface allowing such side reactions to occur.

Consistently, formation of furfuryl alcohol is more favored in aprotic acetone and THF solvents, reaching selectivity virtually twice as higher than furfural (S_{FFA}/S_{FF} = 1.8). Yet a significant amount of unidentified products were formed in acetone (29%), which is probably related to its reaction with intermediate furfural rendering major condensation products as reported elsewhere [41]. GVL, another aprotic solvent, led to a significant production of furfural compared to furfuryl alcohol, presenting the lowest S_{FFA}/S_{FF} ratio of only 0.3. This is in line with some reports

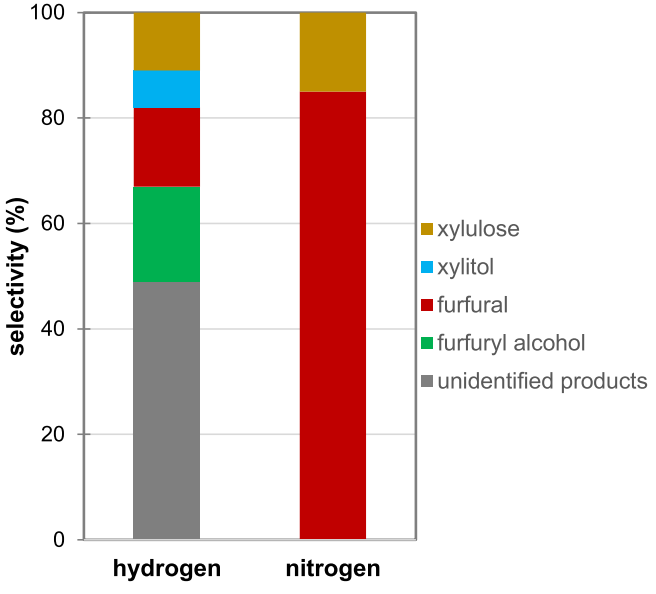

Fig. 5. Selectivity of products over Pt/Nb_2O_5 under hydrogen and nitrogen pressures. Reaction conditions: 130 °C, 30 bar (P_{H2} or P_{N2} = 25 bar), THF:water 1:1, 2 h.

on the remarkable benefits of GVL to dehydrate xylose to furfural [44]. The very low selectivity to furfuryl alcohol may be due to the preferential hydrogenation of C=O bond in GVL instead of that in furfural. Indeed, recent studies have shown that GVL can be hydrogenated under reaction conditions (120 °C, 30 bar) very similar to those applied herein [54].

The performance of Pt/Nb_2O_5 catalyst was finally examined at a longer reaction timeframe. Pd/Nb_2O_5 was also tested due to its equally high selectivity to furfuryl alcohol despite the formation of highly hydrogenated byproducts (Table 1). These time-resolved results are shown in Fig. 6.

As expected, xylose conversion increases along reaction time over both catalysts. Pt/Nb_2O_5 is slightly more active than Pd/Nb_2O_5 as already seen by the initial reaction rates (Table 1) but this trend is switched after 2 h of reaction and Pd/Nb_2O_5 achieves a much higher conversion at 6 h. Selectivity time-dependent curves show that product distribution also varies upon reaction time. Within the first 2 h of reaction, furfuryl alcohol is the main product over both catalysts, however its production dramatically decreases as the reaction proceeds over Pt/Nb_2O_5, reaching around 10% after 6 h. Furfural production, on the other hand, increases steadily (Fig. 6a). It is important to mention that no product was detected from furfuryl alcohol cascade hydrogenation. Its formation drop may then be also associated with its polymerization, which is an acid-catalyzed reaction and reckoned to be thermodynamically favored [55]. Consistently, carbon balance as determined by HPLC analyses was seen to drop as well (Fig. 6). Pd/Nb_2O_5 exhibits a more consistent formation of furfuryl alcohol over time (Fig. 6b). These changes in both conversion and product distribution patterns suggest that a deactivation process is underway, which is more easily distinguished on Pt/Nb_2O_5 (Fig. 6a).

The spent catalysts were then collected after 6 h of reaction and the amount of carbon on them was determined by elemental CHN chemical analysis (Table 3).

As for Pt/Nb_2O_5, additional measurements were performed after 2 and 4 h as well. Residual carbon was indeed found on both catalysts and its content was consistently much higher on Pt/Nb_2O_5, confirming the catalyst deactivates by the deposition of heavy carbon compounds. Eventual contribution from adsorbed reactants is less important as it can be inferred from the minor peak at lower temperature in the complementary thermogravimetric analysis profile of the spent catalyst (Fig. 7). Mass loss due to heavier carbonaceous materials, recorded at higher temperatures, is consistently much more relevant. Furthermore, the carbon content deposited on Pt/Nb_2O_5 was also found to gradually increase upon reaction time. The carbon contents in the freshly reduced catalysts were also determined and they were significantly low as collected in Table 3. It is worth mentioning that the catalysts also turned visibly darker after reaction.

As the formation of furfuryl alcohol is more clearly affected upon carbon deposition (Fig. 6), it could be alleged that the metal sites are the ones more susceptible to deactivation. Deposition of carbonaceous material would cover the metal nanoparticles blocking them and, as a consequence, the hydrogenation ability of the bifunctional catalyst would be expected to decline upon recycling.

A second consecutive reaction cycle was then carried out over Pt/Nb_2O_5. In this experiment, the spent catalyst was used to process a fresh xylose solution and the two reaction cycles are compared in Fig. 8.

Xylose conversion conformingly dropped in the second reaction cycle and product distribution was also seen to change. It is noted, however, that selectivity to metal-catalyzed hydrogenation products, either furfuryl alcohol or xylitol, is virtually the same. Conversely, selectivity to xylulose markedly increased, being twice as much, while to furfural decreased. These findings point then to a different conclusion, unveiling that acid sites are actually the ones suffering from deactivation. Even though it was not possible to assess the acid surface sites after reaction, it may still be suggested that deactivation affects more specifically the Brønsted acid sites. After all, it is well known that those sites are the main responsible for xylose/xylulose dehydration [31] whereas the Lewis acid

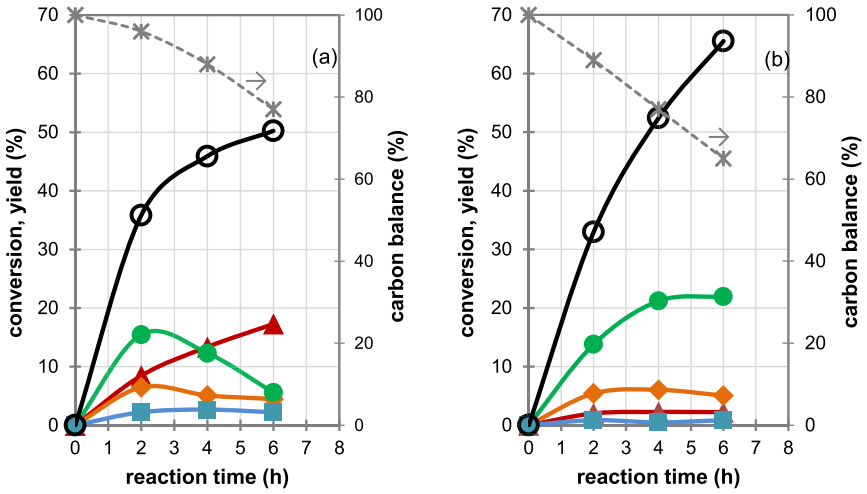

Fig. 6. Time-dependent curves of xylose conversion and products selectivity over Pt/Nb_2O_5 (a) and Pd/Nb_2O_5 (b) catalysts. Reaction conditions: 130 °C, 30 bar (P_{H2} = 25 bar), THF:water 1:1. (○) xylose conversion, (♦) xylulose, (■) xylitol, (▲) furfural, (●) furfuryl alcohol and (*) carbon balance.

Table 3
Carbon content (% C_{CHN}) and concentration of platinum ([Pt]) in the liquid phase after reaction at different times. Reaction conditions: 130 °C, 30 bar (P_{H2} = 25 bar), THF:water 1:1.

Catalyst	Reaction time (h)	%C_{CHN}[a]	[Pt][b] (ppm)
Pt/Nb_2O_5[c]	–	0.27	–
Pt/Nb_2O_5	2	2.70	0.1
Pt/Nb_2O_5	4	3.53	0.3
Pt/Nb_2O_5	6	5.36	0.1
Pd/Nb_2O_5	6	2.19	–
Pd/Nb_2O_5[c]	–	0.24	–

[a] Determined by elementar CHN analysis.
[b] Determined by ICP-OES.
[c] fresh catalyst.

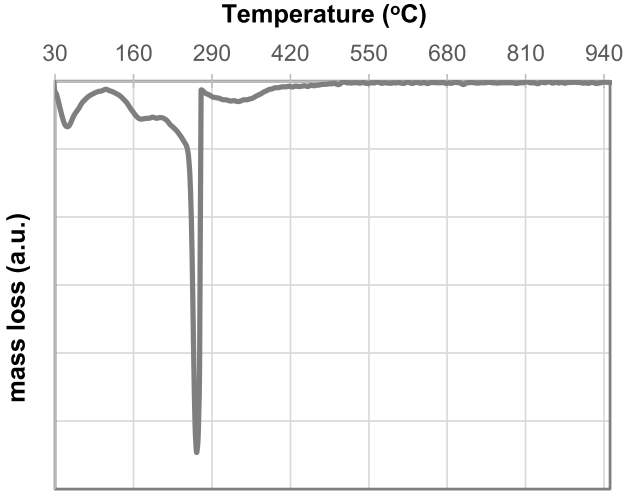

Fig. 7. Derivative thermogravimetric curve of Pt/Nb_2O_5 after reaction.

centers play a role in xylose isomerization to xylulose [31,32], which fits the experimentally observed changes in selectivity displayed in Fig. 8.

From these results pointing to a deactivation process, a new reaction run was carried out but previously regenerating the catalyst. The regenerated sample reached back practically the xylose conversion level and product distribution pattern (Fig. 8).

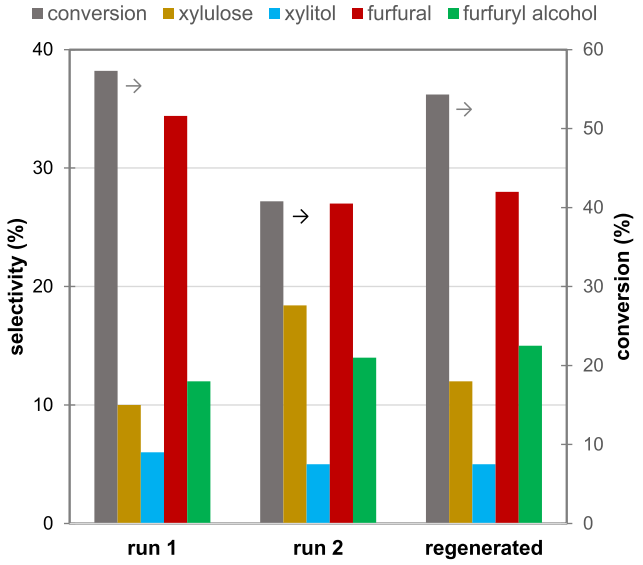

Fig. 8. Xylose conversion and products selectivity over Pt/Nb_2O_5 after two consecutive runs and regeneration of spent catalyst. Reaction conditions: 130 °C, 30 bar (P_{H2} = 25 bar), THF:water 1:1, 6 h.

Chemical stability of Pt/Nb_2O_5 catalyst was assessed by measuring the eventual presence of Pt in the liquid phase after different reaction times (Table 3). Very low concentrations were determined, varying within 0.1–0.3 ppm, which correspond to 0.6–1.8% of all metal in the catalyst, demonstrating that no significant metal leaching occurs upon xylose liquid-phase upgrading over Pt/Nb_2O_5. This result also outlines that the main catalyst deactivation process is indeed the carbonaceous deposits on the catalyst surface.

4. Conclusion

Nb_2O_5-supported platinum-group metals catalysts were shown to be effective bifunctional catalysts for xylose upgrading to bioproducts, promoting isomerization-dehydration-hydrogenation cascade reactions.

Pt/Nb_2O_5 was the best-performing catalyst for xylose upgrading regarding not only xylose consumption rates but also it also led to high selectivity to furfuryl alcohol. Ru, Pd and Rh based catalysts, on the other hand, exhibited a much broader product distribution. Pt/Nb_2O_5 also revealed to be chemically stable for aqueous-phase processing of xylose as no relevant metal leaching was observed. A deactivation process, however, was identified affecting catalyst activity and product distribution in consecutive reaction cycles. This deactivation was attributed to the deposition of carbonaceous materials and it was suggested to disturb the Brønsted acid sites in a more significant way compared to the Lewis and metal surface sites. Catalyst regeneration was shown to be feasible, allowing recovering the same performance. Catalytic activity and the distribution of bioproducts were also found to be determined by the organic solvent:water mixture used as solvent. Polarity was proposed to directly influence catalytic activity whereas intermolecular interactions were suggested to tune selectivity. Protic polar solvents led to a more balanced production of furans (furfural and furfuryl alcohol) while aprotic THF rendered the highest selectivity to furfuryl alcohol.

Funding

This work was supported by CNPq (Proc. 427639/2018-2; Proc. 308146/2019-0) and FAPERJ (E-26/202.660/2019). The authors thank the MCTI/SISNANO/INT-CENANO-CNPq (Proc. 442604/2019) for supporting the STEM analyses.

Declaration of competing interest

Authors declare they have no competing interests.

Acknowledgements

Authors thank CBMM for kindly providing the Nb_2O_5 sample. They are also indebted to Dr. MFL Oliveira from National Institute of Technology – INT for the complementary TGA analysis. PCO thanks CAPES for her scholarship and CRM thanks FAPERJ for the postdoctoral fellowship (E-26/202.395/2021).

References

[1] X. Li, L. Zhang, S. Wang, Y. Wu, Front. Chem. 7 (2020) 1.
[2] A. Susmozas, R. Martín-Sampedro, D. Ibarra, M.E. Eugenio, R. Iglesias, P. Manzanares, A.D. Moreno, Processes 8 (2020) 1.
[3] RenovaBio, Secretary of Petroleum, Natural Gas and Biofuels, Ministry of Mines and Energy, 2021. http://antigo.mme.gov.br/web/guest/secretarias/petroleo-gas-natural-e-biocombustiveis/acoes-e-programas/programas/renovabio. (Accessed 26 July 2021).
[4] R. Roy, M.S. Rahman, D.E. Raynie, Current Research in Green and Sustainable Chemistry 3 (2020) 100035.
[5] L.R.V. Sá, M.O. Faber, A.S.A. Silva, M.C. Cammarota, V.S. Ferreira-Leitão, Renew. Energy 146 (2020) 2408.
[6] R.F. Perez, M.A. Fraga, Green Chem. 16 (2014) 3942.
[7] R.F. Perez, S.J. Canhaci, L.E.P. Borges, M.A. Fraga, Catal. Today 289 (2017) 273.
[8] S.J. Canhaci, R.F. Perez, L.E.P. Borges, M.A. Fraga, Appl. Catal. B Environ. 207 (2017) 279.
[9] R.F. Perez, O.S.G.P. Soares, A.M. Duarte de Farias, M.F.R. Pereira, M.A. Fraga, Appl. Catal. B Environ. 232 (2018) 101.
[10] P.N. Paulino, R.F. Perez, N.G. Figueiredo, M.A. Fraga, Green Chem. 19 (2017) 3759.
[11] T.L. Coelho, B. Marinho, E.M. Alburquerque, M.A. Fraga, Catal. Sci. Technol. 10 (2020) 7071.
[12] E.M. Albuquerque, P.N. Paulino, R. Sadek, L. Valentin, J.M. Krafft, S. Dzwigaj, M.A. Fraga, Appl. Catal. Gen. 604 (2020) 117766.
[13] E.M. Albuquerque, M.A. Fraga, in: M. Brienzo (Ed.), Hemicellulose Biorefinery: A Sustainable Solution for Value Addition to Bio-Based Products and Bioenergy, Springer, 2021.
[14] J. Cui, J. Tan, X. Cui, Y. Zhu, T. Deng, ChemSusChem 9 (2016) 1259.
[15] T. Deng, G. Xu, Y. Fu, Chin. J. Catal. 41 (2020) 404.
[16] G.G. Millán, H. Sixta, Catalysts 10 (2020) 1.
[17] S.G. Wettstein, D. Martin Alonso, E.I. Gürbüz, J.A. Dumesic, Current Opin. Chem. Eng. 1 (2012) 218.
[18] K. Yan, A. Chen, Energy 58 (2013) 357.
[19] A.H. Van Pelt, O.A. Simakova, S.M. Schimming, J.L. Ewbank, G.S. Foo, E.A. Pidko, E.J.M. Hensen, C. Sievers, Carbon 77 (2014) 143.
[20] T. Suoranta, M. Niemelä, P. Perämäki, Talanta 119 (2014) 425.
[21] J. Datka, A.M. Turek, J.M. Jehng, I.E. Wach, J. Catal. 135 (1992) 186.
[22] S.B.T. Tran, H. Choi, S. Oh, J.Y. Park, Catal. Lett. 149 (2019) 2823.
[23] Y. Xin, L. Dong, Y. Guo, X. Liu, Y. Hu, Y. Wang, J. Catal. 375 (2019) 202.
[24] C. García-Sancho, J.M. Rubio-Caballero, J.M. Mérida-Robles, R. Moreno-Tost, J. Santamaría-González, P. Maireles-Torres, Catal. Today 234 (2014) 119.
[25] V.P. Kumar, J.N. Beltramini, S.S. Priya, A. Srikanth, P. Bhanuchander, K.V.R. Chary, Appl. Petrochem. Res. 6 (1) (2016) 73.
[26] A. Piskun, J.G.M. Winkelman, Z. Tang, H.J. Heeres, Catalyst 6 (9) (2016) 131.
[27] S.M.A.H. Siddiki, M.N. Rashed, M.A. Ali, T. Toyao, P. Hirunsit, M. Ehara, K.I. Shimizu, ChemCatChem 11 (2019) 383.
[28] I. Nowak, M. Ziolek, Chem. Rev. 99 (1999) 3603.
[29] K. Skrodczky, M.M. Antunes, X. Han, S. Santangelo, G. Scholz, A.A. Valente, N. Pinna, P.A. Russo, Commun. Chem. 2 (2019) 1.
[30] F. Delbecq, Y. Wang, A. Muralidhara, K.E. El Ouardi, G. Marlair, C. Len, Front. Chem. 6 (2018) 146.
[31] V. Choudhary, S.I. Sandler, D.G. Vlachos, ACS Catal. 2 (2012) 2022.
[32] V. Choudhary, A.B. Pinar, S.I. Sandler, D.G. Vlachos, R.F. Lobo, ACS Catal. 1 (2011) 1724.
[33] T.M. Aida, N. Shiraishi, M. Kubo, M. Watanabe, R.L. Smith, J. Supercrit. Fluids 55 (2010) 208.
[34] O. Ershova, J. Kanervo, S. Hellsten, H. Sixta, RSC Adv. 5 (2015) 66727.
[35] M.J.C. Molina, M.L. Granados, A. Gervasini, P. Carniti, Catal. Today 254 (2015) 90.
[36] N.K. Gupta, A. Fukuoka, K. Nakajima, ACS Catal. 7 (2017) 2430.
[37] Y. Delgado Arcaño, O.D. Valmaña García, D. Mandelli, W.A. Carvalho, L.A. Magalhães Pontes, Catal. Today 344 (2020) 2.
[38] K. Gupta, R.K. Rai, S.K. Singh, ChemCatChem 10 (2018) 2326.
[39] Y. Wang, D. Zhao, D. Rodríguez-Padrón, C. Len, Catalysts 9 (2019) 796.
[40] R. Huang, Q. Cui, Q. Yuan, H. Wu, Y. Guan, P. Wu, ACS Sustain. Chem. Eng. 6 (2018) 6957.
[41] X. Hu, R.J.M. Westerhof, D. Dong, L. Wu, C.Z. Li, ACS Sustain. Chem. Eng. 2 (2014) 2562.
[42] I. Van Zandvoort, Y. Wang, C.B. Rasrendra, E.R.H. Van Eck, P.C.A. Bruijnincx, H.J. Heeres, B.M. Weckhuysen, ChemSusChem 6 (2013) 1745.
[43] G.M. González Maldonado, R.S. Assary, J. Dumesic, L.A. Curtiss, Energy Environ. Sci. 5 (2012) 6981.
[44] M.A. Mellmer, C. Sener, J.M.R. Gallo, J.S. Luterbacher, D.M. Alonso, J.A. Dumesic, Angew. Chem. Int. Ed. 53 (2014) 11872.
[45] R. Srivastava, A. Kumar, ACS Appl. Energy Mater. 3 (2020) 9928.
[46] G. Giorgianni, S. Abate, G. Centi, S. Perathoner, S. Van Beuzekom, S.H. Soo-Tang, J.C. Van Der Waal, ACS Sustain. Chem. Eng. 6 (12) (2018) 16235.
[47] X. Hu, S. Kadarwati, Y. Song, C.Z. Li, RSC Adv. 6 (2016) 4647.
[48] X. Chen, L. Zhang, B. Zhang, X. Guo, X. Mu, Sci. Rep. 6 (2016) 1.
[49] L. Peng, M. Wang, H. Li, J. Wang, J. Zhang, L. He, Green Chem. 22 (2020) 5656.
[50] S. Prakongpan, T. Nagai, Chem. Pharmaceut. Bull. 17 (1984) 340.
[51] D.Y. Murzin, A. Duque, K. Arve, V. Sifontes, A. Atte, K. Eränen, T. Salmi, in: D.Y. Murzin, O.A. Simakova (Eds.), Biomass Sugars for Non-fuel Applications, Royal Society of Chemistry, 2016, p. 265.
[52] J.P. Mikkola, H. Vainio, T. Salmi, R. Sjöholm, T. Ollonqvist, J. Väyrynen, Appl. Catal. Gen. 196 (2000) 143.
[53] D. Zhang, A. Duan, Z. Zhao, X. Wang, G. Jiang, J. Liu, C. Wang, M. Jin, Catal. Today 175 (2011) 477.
[54] I. Simakova, Y. Demidova, M. Simonov, S. Prikhod'ko, P. Niphadkar, V. Bokade, P. Dhepe, D.Y. Murzin, Reactions 1 (2020) 54.
[55] V. Choudhary, A. Pinar, S. Sandler, D. Vlachos, R. Wolf, ACS Catal. 1 (2011) 1724.